RSC Advances

PAPER

View Article Online
View Journal | View Issue

Cite this: *RSC Adv.*, 2018, **8**, 971

Substituent effects of bridged binaphthyl-type chiral dopants on the helical twisting power in dopant-induced chiral liquid crystals†

Yu Narazaki,[a] Hiroya Nishikawa,[b] Hiroki Higuchi,[b] Yasushi Okumura[b] and Hirotsugu Kikuchi*[b]

Received 15th November 2017
Accepted 18th December 2017

DOI: 10.1039/c7ra12465a

rsc.li/rsc-advances

A new series of chiral dopants, (*R*)-6,6′-halogenated (**1b–1e**, X = F, Cl, Br and I) and -methylated (**1f**) binaphthyl compounds, were designed and synthesized to create chiral liquid crystals by doping them into an achiral nematic liquid crystal (NLC). The influence of halogen (X = F, Cl, Br and I) and methyl substituent factors, such as steric, polar, and polarizability properties, on the helical twisting power (HTP) and their temperature dependences on the chiral dopants were investigated in two host NLCs with different characteristics, fluorinated JC-1041XX and *N*-(4-methoxybenzylidene)-4-butylaniline (MBBA). The chiral dopants possessing less steric and larger polarizability factors increased the HTP values. The structural similarity and electrostatic arene–arene interactions between the chiral dopants and the NLC molecules also exerted important influences on these values. The temperature dependence of the HTP ($HTP_{t,d}$) values also correlated well with the steric and polarizability substituents factors in the two host NLCs. Their correlation coefficients (R^2) depended on the molecular structural similarity between the chiral dopant and the NLC.

Introduction

Chirality is a geometric property of chemical structures that indicates a lack of mirror symmetry, and it often induces intriguing physical properties in materials.[1] For example, chiral liquid crystals (CLCs), especially chiral nematic liquid crystals (N*LCs)[2] and blue phase liquid crystals (BPLCs)[3] including polymer-stabilized cholesteric BPLCs,[4] exhibit unusual physical properties, such as periodic helical structures, selective reflections of circularly polarized light based on Bragg's law,[5,6] and a fast electric response.[4,7–9] These CLCs have potential applications in low energy consumption displays[10,11] and tunable optical or laser devices[12–14] because of their unique properties. The development of CLCs or chiral dopants that enable the formation of a N*LC from a nematic liquid crystal (NLC), therefore, has attracted considerable attention. Chiral dopants are asymmetric molecules, and their molecular structures can be classified into four types: central, axial, planar, and helical chirality. The ability of a chiral dopant to generate a helical structure in a given host NLC is evaluated using helical twisting power (HTP), as expressed below:

$$\mathrm{HTP} = (Pc_w)^{-1} \quad (1)$$

where P is the helical pitch of the chiral nematic (N*) phase, and c_w is the concentration of the chiral dopant in weight percentage. Chiral dopants with large HTP values are required for the above-mentioned applications since excess doping of chiral molecule in a host NLC negatively affects the physical properties of induced CLCs.

To date, significant efforts have been devoted to revealing an interrelation between the molecular structure of chiral dopants and the HTP value. For example, studies have been conducted using chiral aryl alkyl carbinol,[15] *trans*-stilbene oxide,[16] binapthyl,[17–19] biphenyl,[20,21] 1-(1-naphthyl)ethylamine,[22] TADDOL (α,α,α,α-tetraaryl-1,3-dioxolane-4,5-dimethanol),[23] 1,2-diphenylethane-1,2-diol,[24] helicene,[25] tartaric imide derivatives[26] and ruthenium complexes possessing octahedral molecular geometry.[27,28] Among them, for several decades, binapthyl-type chiral dopants bridged by an alkyl chain in the 2,2′-position have attracted a great deal of attention both experimentally[17–19] and theoretically[29] since they exhibit a relatively large HTP value in several host NLCs. This means their effective chirality makes them act as solutes to nematic solvent. However, the mechanism of chirality transfer from chiral dopants to host nematics remains unclear. If the mechanism was to be understood on a molecular level, the field of LC science and technology would greatly advance in chemical

[a]*Interdisciplinary Graduate School of Engineering Sciences, Kyushu University, 6-1, Kasuga-koen, Kasuga, Fukuoka 816-8580, Japan*

[b]*Institute for Materials Chemistry and Engineering, Kyushu University, 6-1, Kasuga-koen, Kasuga, Fukuoka 816-8580, Japan. E-mail: kikuchi@cm.kyushu-u.ac.jp*

† Electronic supplementary information (ESI) available: The polarizing optical microscopic images of the contact method of the synthesized chiral dopants, ^{1}H-, ^{13}C, ^{19}F-NMR and high resolution mass spectra of the synthesized chiral dopants. See DOI: 10.1039/c7ra12465a

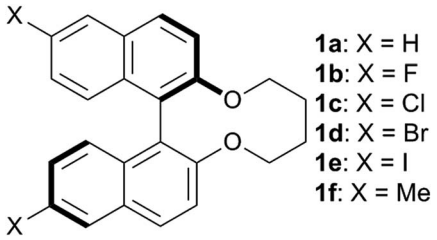

Fig. 1 The chemical structures of synthesized chiral dopants.

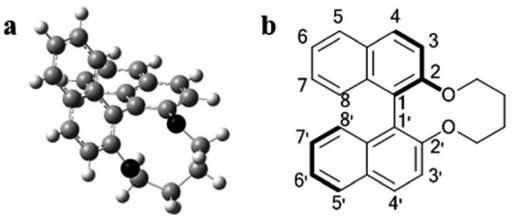

Fig. 2 (a) The optimized structure; (b) the numbering of **1a**.

structure modeling and material design to produce high performance LCs.

In our previous research, the 6,6′-fluorinated binaphthyl-type chiral dopant (**1b**) exhibited a large HTP value, high solubility,[30] and availability of slightly wider blue phase (BP) temperature range[31] in the fluorinated NLC. The effects of fluorine substituents on the HTP value in the induced N*LC phase and the BP temperature range have not yet been well understood. Herein, non-substituted (**1a**), 6,6′-halogenated (**1b–1e**, X = F, Cl, Br and I) and -methylated (**1f**) binaphthyl-type chiral dopants were synthesized to examine dominant molecular factors like the steric hindrance, polarity, and polarizability of their substituents that affect the chirality transfer between the chiral dopant and the host nematic (Fig. 1 and Scheme 1). The effects on the induced HTP due to the substituents in the 6,6′ positions of the binaphthyl-type chiral dopants in two different host NLCs are presented. The binaphthyl-type dopants possessing smaller volumes, larger polarizabilities, and good molecular structural similarities to that of the host NLC exhibited excellent HTP values. Moreover, the electronic states of the aromatic rings of the dopants and the host nematics have a great impact on the HTP values.

Results and discussion

Effect of substituents on dihedral angle of a synthesized binaphthyl-type chiral dopant

The dihedral angle of all of the synthesized chiral dopants was calculated by means of density functional theory (DFT) under the conditions described in Experimental section, and the optimized structure of **1a** is represented in Fig. 2a. According to the DFT calculations, the calculated dihedral angle, θ (C8–C1–C1′–C8′, see Fig. 2b), of **1a**, **1b**, **1c**, **1d**, **1e**, and **1f** were −67.7°, −67.6°, −67.6°, −67.7°, −67.4°, and −67.3°, respectively. The variation in the dihedral angle caused by the different substituents was small even though the sizes of the substituents were different. Additionally, using the contact method, the helical sense of the N*LC induced by the chiral dopant was confirmed to be left-handed for all of the synthesized **1a–1f** compounds in the two host NLCs, JC-1041XX and MBBA, whose dielectric anisotropies were positive and negative, respectively (see the ESI, Fig. S1†).

It is known that the cisoid ($0° < \theta < 90°$) and transoid ($90° < \theta < 180°$) conformations of (*R*)-binaphthyl-type chiral dopants induce the left-handed and the right-handed senses, respectively.[16,17] Therefore, the results of the contact method indicate that the conformations of **1a–1f** adopt a cisoid conformation in the host NLCs. These experimental results agree well with the DFT calculations (θ = 67–68°).

Effects of the substituents on the induced |HTP| value

The absolute HTP values, |HTP|, obtained at the clearing point (T_c) below 5 °C, termed T_c −5 °C, in JC-1041XX and MBBA and three types of substituent parameters that are expected to affect the intermolecular interaction between the chiral dopants and the LC molecules are shown in Table 1. The van der Waals volume parameter (V_{vdw}) corresponds to the steric size of the substituent group.[32] The Hammett constant at the para position (σ_p) indicates an electron-withdrawing or -donating inductive effect of the substituent group.[33] The polarizability (α) is a relative tendency of electric charge distribution of the substituent group, which is calculated as per an equation given in ref. 20.

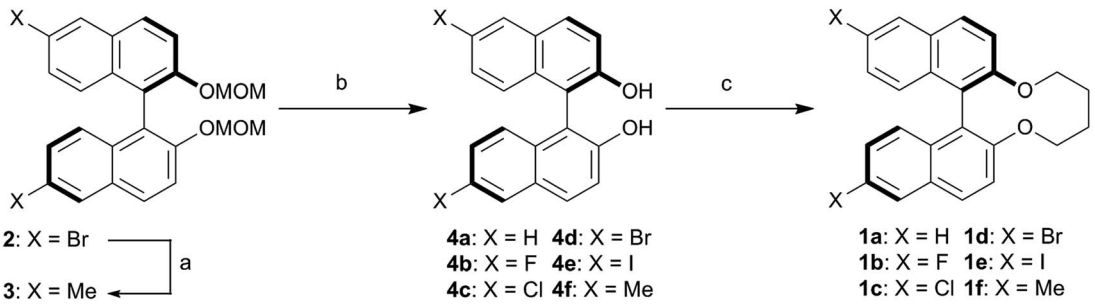

"Key: a) *n*-BuLi, MeI, THF, –78 °C to r.t.; b) 3.0 N methanoic acid, DCM, 0 °C to r.t.; c) K_2CO_3, 1,4-dibromobutane, 18-crown-6, 60 °C."

Scheme 1 Synthetic route for the synthesis of **1a–f**.

Table 1 The |HTP| values of **1a–1f** at T_c −5 °C in JC-1041XX and MBBA and their substituents parameters

		|HTP|/μm^{-1}		Substituent parameters		
Entry	X	JC-1041XX	MBBA	V_{vdw}/ cm mol^{-1}	σ_p	α/ 10^{-23} cm^3
1a	H	49.9	37.1	3.5	0	1.04
1b	F	51.7	46.5	5.8	0.06	1.03
1c	Cl	56.1	48.4	12.0	0.24	1.24
1d	Br	44.9	39.3	15.1	0.27	1.35
1e	I	35.3	30.1	19.6	0.30	1.55
1f	Me	61.7	46.2	13.7	−0.13	1.23

The |HTP| values of **1a–f** in JC-1041XX and MBBA are plotted for substituents of V_{vdw} in Fig. 3a and b to indicate a relationship between the steric effect of their substituents and their |HTP| values. Three trends were found to stand out in the Fig. 3a and b. First, as the substituents volume V_{vdw} increased from 3.5 cm^3 mol^{-1} (X = H) to 12.0 cm^3 mol^{-1} (X = Cl), the |HTP| values tended to increase; however, upon a further increase in the substituents volume to 15.1 cm^3 mol^{-1} (X = Br) and 19.6 cm^3 mol^{-1} (X = I), the |HTP| values decreased. Second, the overall values of **1a–f** in JC-1041XX were larger than those in the MBBA. Third, comparing the |HTP| values of the two host nematics, it was found that the maximum values were for **1f** in JC-1041XX in Fig. 3a and for **1c** in MBBA in Fig. 3b, meaning that the substituents with the highest value was swapped in these two NLCs. In order to understand the causes of those three tendencies, the material parameters affecting the HTPs had to be taken into account.

According to ref. 29, the theoretical HTP equation is expressed as follows:

$$\mathrm{HTP} = RT\varepsilon Q/2\pi K_{22}\nu_m \quad (2)$$

where R is the gas constant; T is the temperature; ε is the orienting strength, which is proportional to the order parameter of the nematic solvent and inversely proportional to temperature;[34] Q is the chirality order parameter, which is a scalar quantity of a helicity tensor ($\boldsymbol{Q}_{ij}$) based on molecular helix and an ordering matrix ($\boldsymbol{S}_{ij}$) of the solute; K_{22} is the twist elastic constant of the host nematic solvent; and ν_m is the molar volume of the solution. This theoretical model, the so-called surface chirality model, is derived from (i) a continuous representation of the twist distortions of the nematic solvent and (ii) a representation of the solute interactions with a type of anchoring energy in the nematic solvents with macroscopic surface. The main chiral intermolecular interaction focused in this study is included in the chirality order parameter Q. A theoretical HTP value and the parameter Q for the binaphthyl-type chiral dopants strongly depend on the dihedral angle (θ) between their two naphthyl planes.[29,35] When a bridged binaphthyl derivative forms a cisoid conformation ($0° < \theta < 90°$), the theoretical HTP should show a maximum value at $\theta = 45°$ (Q is the maximum). By contrast, the helical twisting ability of chiral dopants disappears when θ is 0° and 90° ($Q \approx 0$). In our study, since the dihedral angle of the chiral dopants are almost equivalent to the theoretical DFT calculations as mentioned above, the differences in the observed HTP values for different chiral dopants dissolved in the same nematic LC should be attributed to the influence of the substituents. When comparing the HTP data in different nematic solvent, such as in Fig. 3a and b, the HTP should be normalized by the material parameters depending on the kind of NLC, such as the order parameter included in ε, K_{22} and ν_m. In the data shown in Fig. 3, the measurements were performed at a low temperature, T_c −5 °C, and the effect of the order parameter of the host nematic was small. The influence of ν_m would also be negligible in this study because the dimensions of the JC-1041XX and MBBA molecules are comparable. However, there is a significant difference in K_{22}

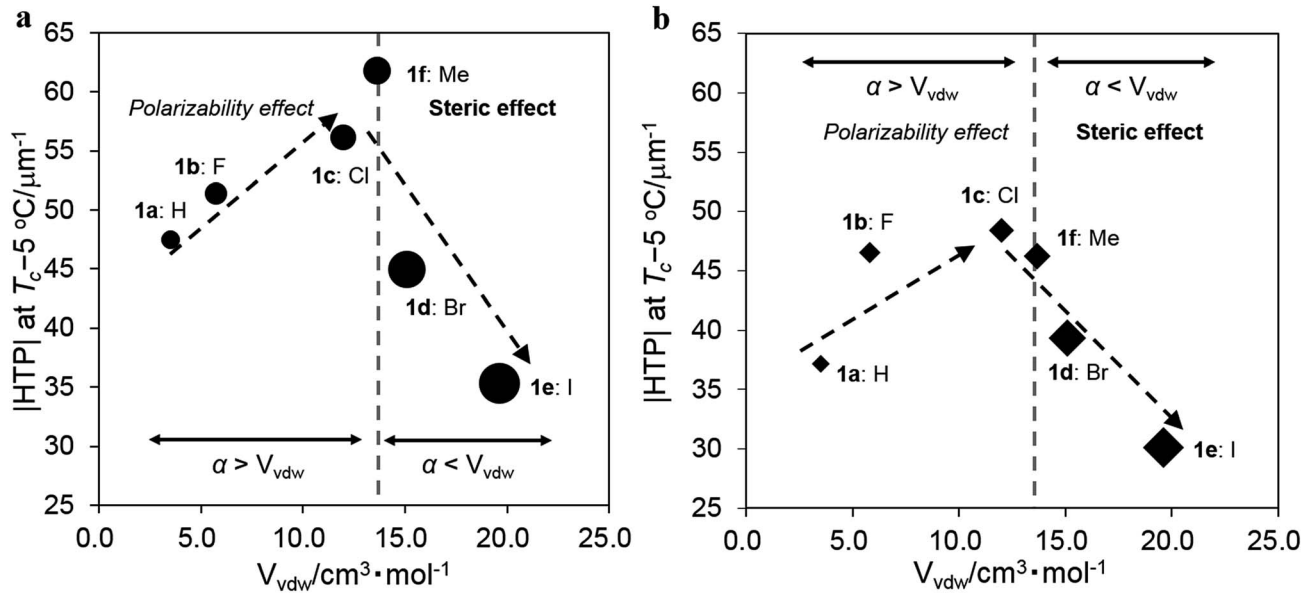

Fig. 3 Plots of the |HTP| values of **1a–f** in (a) JC-1041XX and (b) MBBA *vs.* the V_{vdw} of their substituents.

Table 2 The values of |HTP|K_{22} for **1a–f** at T_c −5 °C in JC-1041XX and MBBA

		$\lvert HTP\rvert K_{22}/10^{-9}$ μm^{-1} N	
Entry	X	JC-1041XX	MBBA
1a	H	4.1	1.6
1b	F	4.3	2.0
1c	Cl	4.7	2.0
1d	Br	3.7	1.7
1e	I	2.9	1.3
1f	Me	5.1	1.9

between the two LCs, 8.3 (ref. 36) and 4.2 (ref. 37) pN for JC-1041XX and MBBA, respectively. Therefore, a normalized |HTP| was calculated using K_{22}, termed |HTP|K_{22}. The values of |HTP|K_{22} are summarized in Table 2. Therefore, it is an intrinsic property that the HTPs of **1a–f** in JC-1041XX are larger than those in the MBBA, as mentioned in trend 2 above.

The possible intermolecular interactions for the three tendencies observed in Fig. 3a and b should be discussed. First, the substituents volume, V_{vdw}, dependences of the |HTP| values showed a maximum of around 13–14 cm^3 mol^{-1} in both JC-1041XX and MBBA. We assume that the steric volume and polarizability effects of the substituents are involved in this phenomenon.

Since both the chiral solute and the host LC solvent have phenyl or naphthyl groups, the arene–arene interaction[38] should be a dominant intermolecular interaction that could regulate the alignment of the molecular axes, by which the twisted molecular alignment of the LC molecules is induced. The intermolecular interactions are mainly governed by a van der Waals interaction in which the polarizability and/or a dipole moment is involved. This means that the interaction should be stronger if a molecule possesses a larger polarizability and/or dipole moment. If the 6,6′ positions of **1a** are replaced by the small-sized halogens, F and Cl, the polarizability and/or the dipole moment of the chiral dopant would be increased. This was seen in the data, where the induced |HTP| values of the chiral dopants possessing smaller substituents increased from non-substituents (X = H) to chlorine (X = Cl) groups. The substituents steric hindrance should have an influence on the intermolecular interaction between the chiral dopants and the host NLC molecules since the arene–arene interactions between them are short-range. Hence, it is reasonable that the weakened intermolecular interactions lead to decrease in the |HTP| values for chiral dopants with large substituents. Furthermore, similar results were already reported with biphenyl[20] and 1,2-diphenylethane-1,2-diol.[24] These studies suggested that lower steric hindrance in the substituents on the phenyl ring plays an important role in inducing a larger HTP value because of the presence of arene–arene interactions between the chiral dopants and the host NLC molecules.

Second, it is important to discuss that the |HTP| values of **1a–f** are larger in the JC-1041XX (Fig. 3a) than in the MBBA (Fig. 3b). The mesogen core of JC-1041XX is biphenyl

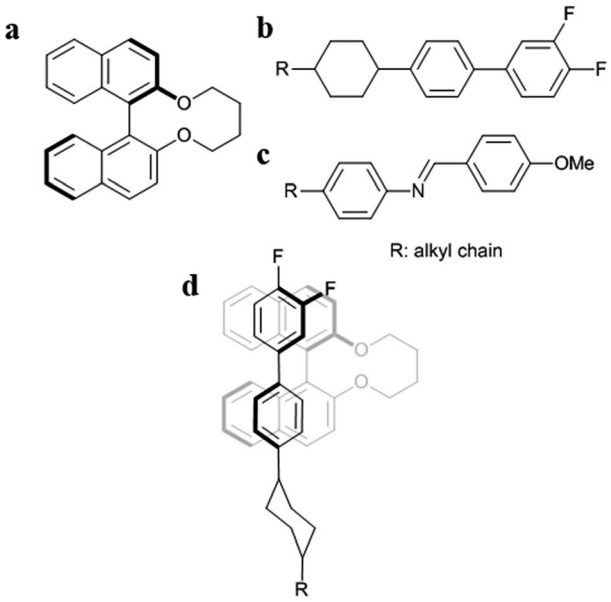

Fig. 4 The chemical structure of (a) a bridged, binaphthyl-type chiral dopant and the mesogenic chemical structures of (b) JC-1041XX and (c) MBBA. (d) The model for the solute–solvent interaction between (a) and (b).

cyclohexane (Fig. 4b); in contrast, the mesogen core of MBBA is azomethine (Fig. 4c). The length of the aromatic unit at the core of JC-1041XX corresponds to the surface of a bridged binaphthyl-type chiral dopant (Fig. 4a), particularly in comparison with the core of the MBBA. JC-1041XX, which has a higher structural similarity to its dopant than MBBA, should interact well with the chiral dopants. This is seen in the larger |HTP| values for **1a–f** in JC-1041XX than that for in the MBBA. Gottarelli *et al.* (1983) proposed the model for the solute–solvent interaction between the bridged binaphthyl-type chiral solute and the host NLC solvent (Fig. 4d). The model indicates that the structural similarity between the chiral solutes and the host NLC solvents leads to a larger HTP value. The HTP values for bridged binaphthyl-type chiral dopants tend to be larger in the biphenyl-type NLC, such as 5CB and E7, than that in the MBBA[17,19] because both the dopant and the NLC have a biphenyl core. Therefore, it is reasonable that such a strong intermolecular interaction between chiral dopants and host NLC molecules contribute to chiral transfer.

Third, the relationship between the |HTP| values for **1c** (X = Cl) and **1f** (X = Me) was reversed between JC-1041XX (Fig. 3a) and MBBA (Fig. 3b). The steric and polarizability parameters (V_{vdw} and α) are almost similar between **1c** and **1f**. Conversely, the signs of the Hammett constant at the para position, σ_p, of **1c** and **1f** are the opposite, *i.e.*, positive for **1c** and negative for **1f**. JC-1041XX and MBBA bear one part of an electron withdrawing and donating aromatic ring, respectively. The electronic states of the aromatic rings of **1f** and JC-1041XX are electron rich and electron deficient, respectively. In contrast, those of **1c** and MBBA are electron deficient and electron rich, respectively. The combination of the electron-rich and -deficient aromatic rings can lead to favorable arene–arene interactions.[39] Additionally, the

Table 3 The $HTP_{t.d.}$ values for **1a–1f** in JC-1041XX and MBBA and their substituents parameters

		$HTP_{t.d.}$/% T^{-1}		Substituent parameters		
Entry	X	JC-1041XX	MBBA	V_{vdw}/ cm mol^{-1}	σ_p	α/ 10^{-23} cm^3
1a	H	0.46	0.49	3.5	0	1.04
1b	F	0.43	0.73	5.8	0.06	1.03
1c	Cl	0.59	0.85	12.0	0.24	1.24
1d	Br	0.60	0.87	15.1	0.27	1.35
1e	I	0.69	0.87	19.6	0.30	1.55
1f	Me	0.64	0.82	13.7	−0.13	1.23

strong solute–solvent molecular interaction between the chiral dopants and the nematic solvents is known to enhance the HTP value.[40] This explains why the |HTP| values were maximized for **1f** in JC-1041XX (Fig. 3a) and **1c** in MBBA (Fig. 3b).

Substituent effect on the temperature dependence of the HTP value

Unlike pure cholesterol materials, the pitch of induced N* doped with **1a–f** increases as a function of temperature, *i.e.*, the |HTP| values decrease with increase in the temperature. An HTP temperature dependence value ($HTP_{t.d.}$) was defined as below:

$$HTP_{t.d.} = (\Delta HTP/\overline{HTP})/\Delta T \times 100 \quad (3)$$

where ΔHTP is the difference between the maximum and minimum |HTP| values, and $\overline{HTP}$ is the arithmetic mean of the |HTP| values in the temperature range from T–T_c = −5 to 25 °C.[30,41] The index indicates the percentage change in the |HTP| values per 1 °C.[30,41] The $HTP_{t.d.}$ values for **1a–1f** and their substituents parameters are shown in Table 3. The $HTP_{t.d.}$ values for **1a–f** in (a) JC-1041XX and (b) MBBA are plotted against their steric (V_{vdw}) and polarizability (α) substituents

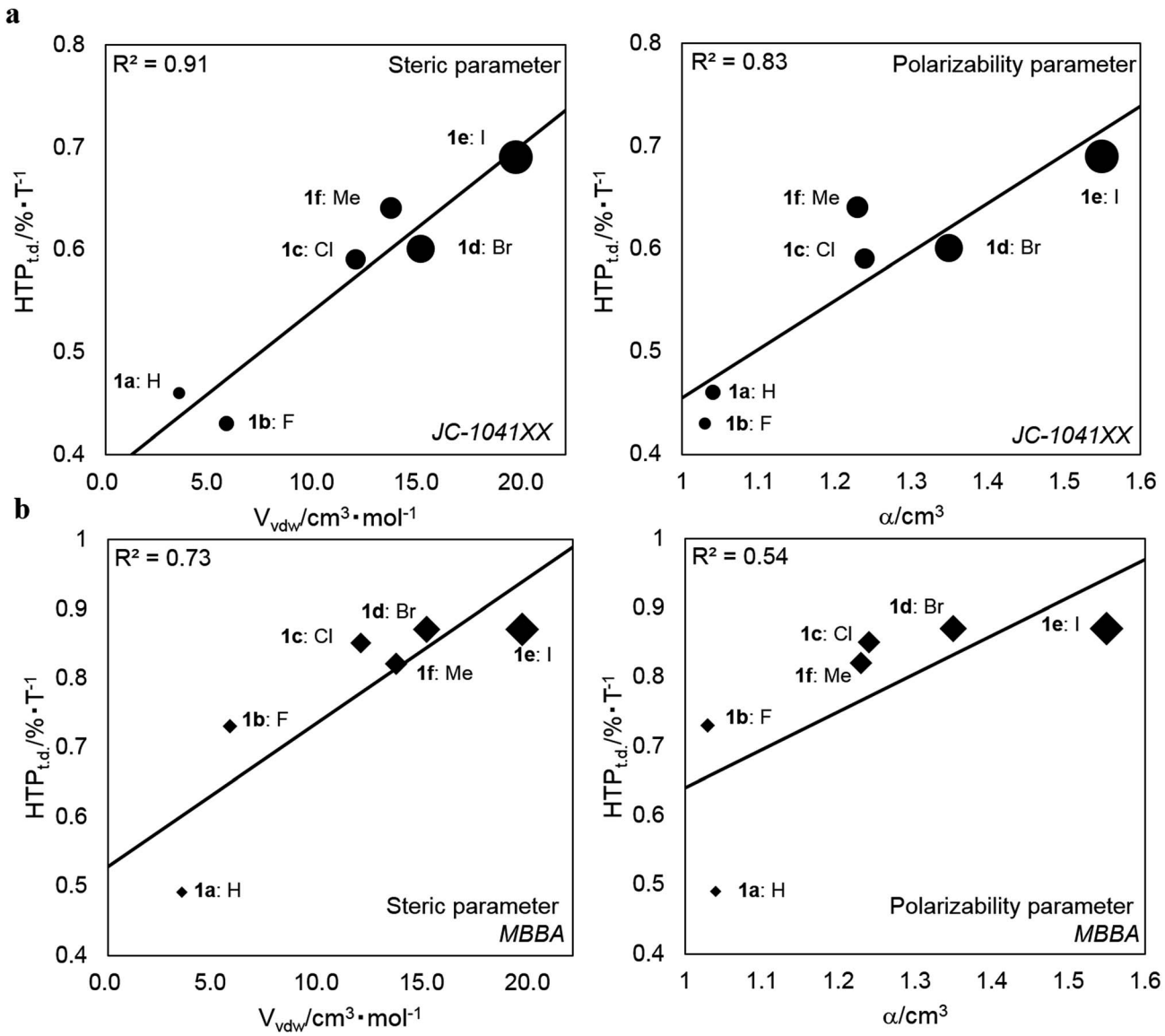

Fig. 5 Plots of the $HTP_{t.d.}$ values for **1a–1f** against the V_{vdw} and α of their substituents in (a) JC-1041XX and (b) MBBA. R^2 denotes the correlation coefficient.

parameters in Fig. 5a and b to evaluate the effect of the substituents on their subsequent $HTP_{t.d.}$ values.

As shown in Fig. 5a and b, the $HTP_{t.d.}$ values increased with increasing V_{vdw} and α. This trend was especially clear in JC-1041XX, more so than in MBBA. In addition, the $HTP_{t.d.}$ values in MBBA were larger than those in JC-1041XX. When the host NLC was JC-1041XX, the correlation coefficients (R^2) for the steric and polarizability parameters were 0.91 and 0.83, respectively. Those same in parameters had correlations of 0.73 and 0.54, respectively, in MBBA. From these results, it is clear that the $HTP_{t.d.}$ values and R^2 values in JC-1041XX were better than those in MBBA. It is appropriate that molecular structural similarity of a solute–solvent interaction between a bridged chiral solute and host nematic solvent can affect the $HTP_{t.d.}$ and R^2 values. It is assumed that the structural similarity between the chiral solutes and MBBA might cause the resultant LCs to thermally disintegrate faster than in JC-1041XX.

In comparison with the $HTP_{t.d.}$ values in the two host nematics with their steric and polarizability substituents parameters, it became clear that the $HTP_{t.d.}$ values correlated well with their substituents parameters. Our understanding is that a van der Waals interaction involving polarizability can impact the $HTP_{t.d.}$ values of the smaller substituents of synthesized chiral dopants, such as **1a–c** and **1f**, because these $HTP_{t.d.}$ values gradually increase as their polarizability increased. Moreover, the steric substituents effects of the relevant chiral dopants on $HTP_{t.d.}$ values were observed; chiral dopants possessing larger substituents, such as the bromo and iodo groups, promoted a disaggregation of the arene–arene interactions between these chiral dopants and the host NLC molecules. This could be because the steric hindrance between them should affect their short-range interactions. This effect should be reflected the $HTP_{t.d.}$ values of **1d–e**, since these values were comparatively larger than those of **1a–c** and **1f** in the two host NLCs. Therefore, the 6,6′ substituents of synthesized chiral dopants also affect their $HTP_{t.d.}$ values.

Conclusions

Our systematic studies of the 6,6′-substituted bridged, binaphthyl-type chiral dopants suggested that the induced |HTP| and $HTP_{t.d.}$ values were significantly dependent on the arene–arene interactions between the chiral dopants and the host nematic NLCs. Furthermore, their interactions were affected by the steric hindrance, aromatic ring polarity, and polarizability of the substituents. The bridged binaphthyl-type chiral dopant with the least steric hindrance and a largest substituents polarizability, the 6,6′-chlorinated chiral dopant, exhibited large |HTP| values in both host NLCs since the chlorine group has an adequate substituents volume and large polarizability that contribute to a strong arene–arene interaction between the dopants and the host NLC molecules. Moreover, the aromatic polarity of the chiral dopants and host NLCs exerted a beneficial impact on the induced |HTP| values to give a strong electrostatic arene–arene interaction between them. In $HTP_{t.d.}$ investigations, the $HTP_{t.d.}$ values depended upon the structural similarity of a solute–solvent interaction between the chiral solutes and host nematic solvents. Structural similarity between the synthesized chiral dopants and biphenyl cyclohexane type NLC, JC-1041XX, lead to smaller $HTP_{t.d.}$ values, indicating a better thermal property for a chiral dopant. By contrast, the values between the chiral dopants and azomethine-type NLC, MBBA, exhibited larger $HTP_{t.d.}$ values, meaning they displayed a lesser stability toward heat. Furthermore, the $HTP_{t.d.}$ values were affected by the steric and polarizability substituents parameters since the $HTP_{t.d.}$ values in the two host NLCs had a good correlation with their substituents parameters. Our understanding is that when substituents polarizability are larger, which is relevant for a van der Waals interaction between the chiral dopants and the NLC molecules, the $HTP_{t.d.}$ values for the smaller substituents increase. In the case of larger substituents, such as bromo and iodo groups, the $HTP_{t.d.}$ values are considerably larger because of a disaggregation of the arene–arene interactions between these chiral dopants and the host NLCs *via* steric hindrance. We believe that our results presented herein significantly advance the design of novel binaphthyl-type chiral dopants with larger HTP values.

Experimental

General

(*R*)-6,6′-Dibromo-2,2′-bis(methoxymethoxy)-1,1′-binaphthalene (**2**), (*R*)-6,6′-difluoro-2,2′-dihydroxy-1,1′-binaphthalene (**4b**), (*R*)-6,6′-dichloro-2,2′-dihydroxy-1,1′-binaphthalene (**4c**), (*R*)-6,6′-dibromo-2,2′-dihydroxy-1,1′-binaphthalene (**4d**) and (*R*)-6,6′-diiodo-2,2′-dihydroxy-1,1′-binaphthalene (**4e**) were prepared as reported previously.[42,43] All of reagents and solvents were purchased from Aldrich Chemical Co., Kanto Chemical Co., Inc., Tokyo Chemical Industry Co., Ltd. and Wako Pure Chemical Industries, Ltd. and used without further purification. Analytical thin layer chromatography (TLC) was performed on silica gel layer glass plate Merck 60 F_{254} and visualized by UV irradiation (254 nm). Column chromatography was undertaken on Wako Pure Chemical Industries, Ltd. Wakogel 60N 63–212 μm or Wakogel C-400HG 20–40 μm. ^{1}H- and ^{13}C-NMR spectra were recorded on JEOL JNM-LA 400 and JNM-ECA 600 with the TMS (trimethylsilane) as an internal standard for ^{1}H and the deuterated solvent for ^{13}C. ^{19}F-NMR spectra were recorded on JEOL ECZ 400 with the benzotrifluoride as an internal standard. Chemical shift (δ) was expressed in parts-per million (ppm) to relative internal standards. Signal multiplicities were abbreviated by s (singlet), d (doublet), t (triplet), q (quartet), dd (double–doublet), br (broad) and m (multiplet), respectively. High resolution mass spectra were performed on JEOL JNM-700. Elemental analyses were made on YANACO CHN-recorder MT-5 or YANACO CHN-recorder MT-6. Polarized optical microscopy was performed on Nikon ECLIPSE E600 POL equipped with Zeiss AxioCam HRc as a high-resolution camera. The temperature of the samples was controlled using the heating stage Linkam LTS420E with Linkam 10084L controller. The geometry optimizations of all synthesized chiral dopants were calculated using B3LYP/6-31G(d) for **1a**, **1b**, **1c**, **1d** and **1f** and B3LYP/Gen basis set for the iodo atom of **1e** level of density function theory (DFT) *via* the Gaussian 09 program.[44]

Synthesis

Synthesis of (*R*)-6,6′-dimethyl-2,2′-bis(methoxymethoxy)-1,1′-binaphthalene (3). To a solution of (*R*)-6,6′-dibromo-2,2′-bis(methoxymethoxy)-1,1′-binaphthalene **2** (8.0 g, 15 mmol) in anhydrous THF (80 mL), *n*-BuLi in hexane (*ca.* 1.6 M, 28 mL, 45 mmol) was added slowly dropwise under argon atmosphere at −78 °C. After stirring for 0.5 h at −78 °C, a solution of methyl iodide (2.8 mL, 45 mmol) in anhydrous THF (10 mL) was added to the mixture at −78 °C and then the reaction mixture was gradually allowed to warm to room temperature. After stirring for over 12 h at room temperature, the resulting mixture was extracted with EtO_2 (3 × 50 mL). The ethereal extracts were washed with sat. $NaHCO_3$ aq solution (50 mL), water (50 mL), 10% sodium thiosulfate aq solution (50 mL) and brine (50 mL), dried over $MgSO_4$ and evaporated. The crude product was purified by silica-gel chromatography (DCM/*n*-heptane = 1/1, v/v%) to afford **3** (5.6 g, 93%) as a white viscous powder; ^{1}H-NMR (400 MHz, $CDCl_3$) δ 7.85 (d, J = 8.8 Hz, 2H), 7.63 (br s, 2H), 7.52 (d, J = 8.8 Hz, 2H), 7.05 (br s, 4H), 5.04 (d, J = 6.8 Hz, 2H), 4.94 (d, J = 6.8 Hz, 2H), 3.14 (s, 6H), 2.45 (s, 6H); ^{13}C-NMR (100 MHz, $CDCl_3$) δ 152.08, 133.53, 132.22, 130.15, 128.57, 126.82, 125.48, 121.54, 117.65, 95.46, 55.80, 21.40 (one ^{13}C signal derived from its naphthyl ring could not be observed since the signal might be overlapped with the other ^{13}C signals of the naphthyl ring); HRMS (EI) calcd for $C_{26}H_{26}O_4$ [M^+] 402.1831, found 402.1831.

Synthesis of (*R*)-6,6′-dimethyl-2,2′-dihydroxy-1,1′-binaphthalene (4f). To a solution of (*R*)-6,6′-dimethyl-2,2′-bis(methoxymethoxy)-1,1′-binaphthalene **4** (5.6 g, 14 mmol) in anhydrous DCM (5 mL), methanoic acid (3.0 N, 10 mL, 30 mmol) was added dropwise under argon atmosphere at 0 °C. After stirring for 3 h at room temperature, the reaction mixture was evaporated and diluted with DCM (50 mL). The organic layer was washed with sat. $NaHCO_3$ aq solution (50 mL), water (50 mL) and brine (50 mL), dried over $MgSO_4$ and evaporated. The crude product was purified by silica-gel chromatography (EtOAc/*n*-heptane = 2/8, v/v%) and then recrystallization from DCM/*n*-heptane to afford **4f** (2.8 g, 64%) as a white crystal; ^{1}H-NMR (400 MHz, $CDCl_3$) δ 7.88 (d, J = 9.8 Hz, 2H), 7.66 (br s, 2H), 7.34 (d, J = 8.8 Hz, 2H), 7.14 (dd, J = 2.0 Hz, J = 2.0 Hz, 2H), 7.05 (d, J = 8.8 Hz, 2H), 4.96 (s, 2H), 2.46 (s, 6H); ^{13}C-NMR (100 MHz, $CDCl_3$) δ 152.02, 133.56, 131.51, 130.64, 129.65, 129.64, 127.47, 124.13, 117.70, 110.85, 21.31; HRMS (EI) calcd for $C_{22}H_{18}O_2$ [M^+] 314.1307, found 314.1308.

General procedure of (*R*)-closed binaphthyl type chiral dopants

A solution of **4a–b** (1 equiv.), 18-crown-6 (catalytical quantity), and K_2CO_3 (2.2 equiv.) in acetone (100 mL per 1 mmol of (*R*)-6,6′-substituted-2,2′-dihydroxy-1,1′-binaphthalene) was refluxed under argon atmosphere at 60 °C. After refluxing for 2 h at 60 °C, a solution of 1,4-dibromobutane (1.1 equiv.) in acetone (15.5 mL per 1 mmol of 1,4-dibromobutane) was slowly added to the refluxing solution for over 8 h by using syringe pump and then the resulting mixture was refluxed for 120 h at 60 °C. After cooling, the reaction mixture was filtered out and evaporated. The residue was diluted with water and extracted with Et_2O (2 × 50 mL). The ethereal extracts were washed with water (50 mL) and brine (50 mL), dried over $MgSO_4$ and evaporated. The crude product was purified by silica-gel chromatography (DCM/hexanes) and then recrystallization from EtOH or DCM/hexanes to afford the titled compounds.

1a. According to the general procedure. The crude product was purified by silica-gel chromatography (DCM/hexanes = 3/7, v/v%), followed by recrystallization from DCM/hexanes to afford **1a** (587 mg, 58%) as a white crystal; ^{1}H-NMR (400 MHz, $CDCl_3$) δ 7.95 (d, J = 8.8 Hz, 2H), 7.86 (d, J = 8.8 Hz, 2H), 7.49 (d, J = 8.8 Hz, 2H), 7.32 (t, J = 7.8 Hz, J = 6.8 Hz, 2H), 7.19 (t, J = 8.8 Hz, J = 6.8 Hz, 2H), 7.09 (d, J = 8.8 Hz, 2H), 4.55–4.51 (m, 2H), 4.11 (t, J = 9.8 Hz, J = 10.8 Hz, 2H), 1.88–1.71 (m, 4H); ^{13}C-NMR (100 MHz, $CDCl_3$) δ 153.30, 134.12, 129.83, 129.36, 127.95, 126.37, 125.81, 123.97, 122.39, 117.41, 70.36, 25.31; elemental anal. calcd for $C_{24}H_{20}O_2$ C 84.68, H 5.92, found C 84.65, H 5.96; HRMS (EI) calcd for $C_{24}H_{20}O_2$ [M^+] 340.1463, found 340.1463.

1b. According to the general procedure. The crude product was purified by silica-gel chromatography (DCM/hexanes = 2/8, v/v%), followed by recrystallization from EtOH to afford **1b** (234 mg, 41%) as a white crystal; ^{1}H-NMR (400 MHz, $CDCl_3$) δ 7.88 (d, J = 9.8 Hz, 2H), 7.51 (d, J = 8.8 Hz, 2H), 7.48 (dd, J = 9.7 Hz, J = 2.9 Hz, 2H), 7.05–6.96 (m, 4H), 4.50 (d, J = 11.7 Hz, 2H), 4.12 (t, J = 10.8 Hz, J = 11.7 Hz, 2H), 1.86–1.71 (m, 4H); ^{13}C-NMR (150 MHz, $CDCl_3$) δ 180.34 (d, J = 303.4 Hz), 171.73, 144.44, 143.74 (d, J = 10.8 Hz), 141.67 (d, J = 5.4 Hz), 140.77 (d, J = 10.8 Hz), 133.80, 129.12, 126.64 (d, J = 30.5 Hz), 119.51 (d, J = 25.1 Hz), 68.90, 12.29; ^{19}F-NMR (376 MHz, $CDCl_3$) −119.12 (m, 2F); elemental anal. calcd for $C_{24}H_{18}F_2O_2$ C 76.58, H 4.82, found C 76.91, H 4.86; HRMS (EI) calcd for $C_{24}H_{18}F_2O_2$ [M^+] 376.1275, found 376.1275.

1c. According to the general procedure. The crude product was purified by silica-gel chromatography (DCM/hexanes = 3/7, v/v%), followed by recrystallization from EtOH to afford **1c** (666 mg, 54%) as a white crystal; ^{1}H-NMR (400 MHz, $CDCl_3$) δ 7.87 (d, J = 8.8 Hz, 2H), 7.84 (d, J = 2.0 Hz, 2H), 7.51 (d, J = 8.8 Hz, 2H), 7.14 (dd, J = 2.0 Hz, J = 6.8 Hz, J = 3.0 Hz, 2H), 6.99 (d, J = 8.8 Hz, 2H), 4.50 (d, J = 11.6 Hz, 2H), 4.13 (t, J = 10.1 Hz, 2H), 1.86–1.73 (m, 4H); ^{13}C-NMR (100 MHz, $CDCl_3$) δ 153.69, 132.24, 130.39, 129.87, 128.72, 127.33, 127.26, 126.68, 121.96, 118.52, 70.51, 25.39; elemental anal. calcd for $C_{24}H_{18}Cl_2O_2$ C 70.43, H 4.43, found C 70.47, H 4.43; HRMS (EI) calcd for $C_{24}H_{18}Cl_2O_2$ [M^+] 408.0684, found 408.0684.

1d. According to the general procedure. The crude product was purified by silica-gel chromatography (DCM/hexanes = 3/7, v/v%), followed by twice recrystallization from EtOH to afford **1d** (410 mg, 28%) as a white crystal; ^{1}H-NMR (400 MHz, $CDCl_3$) δ 8.02 (d, J = 2.0 Hz, 2H), 7.86 (d, J = 9.8 Hz, 2H), 7.50 (d, J = 9.8 Hz, 2H), 7.26 (dd, J = 2.0 Hz, J = 7.8 Hz, 2H), 6.92 (d, J = 9.8 Hz, 2H), 4.50 (d, J = 10.8 Hz, 2H), 4.13 (t, J = 8.8 Hz, J = 10.7 Hz, 2H), 1.87–1.73 (m, 4H); ^{13}C-NMR (100 MHz, $CDCl_3$) δ 153.79, 132.44, 130.87, 129.98, 129.79, 128.71, 127.37, 121.91, 118.45, 117.98, 70.49, 25.40; elemental anal. calcd for $C_{24}H_{18}Br_2O_2$ C 57.86, H 3.64, found C 57.77, H 3.59; HRMS (EI) calcd for $C_{24}H_{18}Br_2O_2$ [M^+] 495.9674, found 495.9673.

1e. According to the general procedure. The crude product was purified by silica-gel chromatography (DCM/hexanes = 3/7,

v/v%), followed by recrystallization from DCM/hexanes to afford **1e** (306 mg, 48%) as a white powder; ^{1}H-NMR (400 MHz, $CDCl_3$) δ 8.24 (d, J = 1.9 Hz, 2H), 7.83 (d, J = 8.8 Hz, 2H), 7.48 (d, J = 9.8 Hz, 2H), 7.41 (dd, J = 2.0 Hz, J = 6.8 Hz, 2H), 6.78 (d, J = 8.8 Hz, 2H), 4.50 (d, J = 11.7 Hz, 2H), 4.12 (t, J = 8.8 Hz, J = 10.8 Hz, 2H), 1.85–1.71 (m, 4H); ^{13}C-NMR (100 MHz, $CDCl_3$) δ 153.93, 136.65, 134.93, 132.76, 131.743, 128.57, 127.34, 121.83, 118.21, 89.27, 70.46, 25.43; elemental anal. calcd for $C_{24}H_{18}I_2O_2$ C 48.68, H 3.06, found C 48.74, H 2.99; HRMS (EI) calcd for $C_{24}H_{18}I_2O_2$ [M^+] 591.9396, found 591.9395.

1f. According to the general procedure. The crude product was purified by silica-gel chromatography (DCM/hexanes = 1/1, v/v%), followed by recrystallization from EtOH to afford **1f** (382 mg, 35%) as a colorless crystal; ^{1}H-NMR (400 MHz, $CDCl_3$) δ 7.84 (d, J = 8.8 Hz, 2H), 7.62 (s, 2H), 7.44 (d, J = 9.8 Hz, 2H), 7.02 (dd, J = 1.9 Hz, J = 2.0 Hz, 2H), 6.98 (d, J = 8.8 Hz, 2H), 4.49 (d, J = 11.7 Hz, 2H), 4.08 (t, J = 9.8 Hz, J = 11.7 Hz, 2H), 2.43 (s, 6H), 1.86–1.82 (m, 2H), 1.74–1.68 (m, 2H); ^{13}C-NMR (100 MHz, $CDCl_3$) δ 152.56, 133.40, 132.33, 130.03, 128.62, 128.57, 126.90, 125.67, 122.57, 117.55, 70.33, 25.18, 21.35; elemental anal. calcd for $C_{26}H_{24}O_2$ C 84.75, H 6.57, found C 84.83, H 6.53; HRMS (EI) calcd for $C_{26}H_{24}O_2$ [M^+] 368.1776, found 368.1778.

Measurement of synthesized chiral dopants' HTP

Synthesized chiral dopants were dissolved in host NLCs. JC-1041XX, which is a fluorinated nematic mixture supplied by JNC Co., and *N*-(4-methoxybenzylidene)-4-butylaniline (MBBA) were used as 0.5 wt% sample solutions. Prepared solutions were stirred at their isotropic phase temperature for three hours and were injected in a Grandjean–Cano wedge-shaped cell (E. H. C. Co., KCRK-03, tan θ = 0.0079 ± 10%). After cooling to a N* phase, the interval distances of the striped defect lines that appeared in the cell were measured at temperatures well below the clearing point (T_c), T_c −5 °C, −10 °C, −15 °C, −20 °C, and −25 °C, in JC-1041XX and MBBA by means of a polarizing optical microscope. Measurements were repeated three times, and their given HTP values were averaged.

Identification of the helical sense of the synthesized chiral dopants

The helical sense of the synthesized chiral dopants was determined by a contact method using cholesteryl oleyl carbonate (COC) as a reference material. The 0.5 wt% samples doped with chiral dopants were injected from one side of the Grandjean–Cano wedge-shaped cell, and the COC was injected from the other side of its cell. After being in static for several hours, the helical sense was determined by polarizing optical microscopy.

Conflicts of interest

There are no conflicts to declare.

Acknowledgements

This work was performed under the Advanced Graduate Program in Global Strategy for Green Asia, Kyushu University. The authors thank to K. Ideta (Kyushu University, Institute for Materials Chemistry and Engineering) for valuable discussion on ^{13}C-NMR spectroscopy. This work was partially supported by a Grant-in-Aid for Scientific Research (A) JSPS KAKENHI Grant Number JP25248021 from the Japan Society for the Promotion of Science, Dynamic Alliance for Open Innovation Bridging Human, Environment and Materials from the Ministry of Education, Culture, Sports, Science and Technology, Japan (MEXT), the Cooperative Research Program of "Network Joint Research Center for Materials and Devices." and CREST, JST (JPMJCR1424).

Notes and references

1 I. Dierking, *Symmetry*, 2014, **6**, 444–472.
2 G. Solladié and R. G. Zimmermann, *Angew. Chem., Int. Ed. Engl.*, 1984, **23**, 348–362.
3 D. C. Wright and N. D. Mermin, *Rev. Mod. Phys.*, 1989, **61**, 385–432.
4 H. Kikuchi, M. Yokota, Y. Hisakado, H. Yang and T. Kajiyama, *Nat. Mater.*, 2002, **1**, 64–68.
5 S. Shibayama, H. Higuchi, Y. Okumura and H. Kikuchi, *Adv. Funct. Mater.*, 2013, **23**, 2387–2396.
6 H. K. Bisoyi and Q. Li, *Acc. Chem. Res.*, 2014, **47**, 3184–3195.
7 Y. Hisakado, H. Kikuchi, T. Nagamura and T. Kajiyama, *Adv. Mater.*, 2005, **17**, 96–98.
8 S. Yabu, H. Yoshida, G. Lim, K. Kaneko, Y. Okumura, N. Uehara, H. Kikuchi and M. Ozaki, *Opt. Mater. Express*, 2011, **1**, 1577–1584.
9 H. Choi, H. Higuchi and H. Kikuchi, *Soft Matter*, 2011, **7**, 4252–4256.
10 Y. Hirakata, D. Kubota, A. Yamashita, H. Miyake, M. Hayakawa, J. Koyama, S. Yamazaki, K. Okazaki, R. Sato, T. Cho, K. Tochibayashi and M. Sakakura, *SID'11 Digest*, 2011, vol. 42, pp. 32–35.
11 J. Chen and C. T. Liu, *IEEE Access*, 2013, **1**, 150–158.
12 M. Ozaki, Y. Matsuhisa, H. Yoshida, R. Ozaki and A. Fujii, *Phys. Status Solidi A*, 2007, **204**, 3777–3789.
13 W. Cao, A. Muñoz, P. Palffy-Muhoray and B. Taheri, *Nat. Mater.*, 2002, **1**, 111–113.
14 S. Yokoyama, S. Mashiko, H. Higuchi, K. Uchida and T. Nagamura, *Adv. Mater.*, 2006, **18**, 48–51.
15 G. Gottarelli, B. Samori, C. Stremmenos and G. Torre, *Tetrahedron*, 1981, **37**, 395–399.
16 G. Gottarelli, P. Mariani, G. P. Spada, B. Samori, A. Forni, G. Solladie and M. Hobert, *Tetrahedron*, 1983, **39**, 1337–1344.
17 G. Gottarelli, M. Hobert, B. Samori, G. Solladié, G. P. Spada and R. Zimmermann, *J. Am. Chem. Soc.*, 1983, **105**, 7318–7321.
18 H.-J. Deuβen, P. V. Shibaev, R. Vinokur, T. Bjørnholm, K. Schaumburg, K. Bechgaard and V. P. Shibaev, *Liq. Cryst.*, 1996, **21**, 327–340.
19 G. Proni and G. P. Spada, *J. Org. Chem.*, 2000, **65**, 5522–5527.
20 V. E. Williams and R. P. Lemieux, *Chem. Commun.*, 1996, 2259–2260.
21 A. di Matteo, S. M. Todd, G. Gottarelli, G. Solladié, V. E. Williams, R. P. Lemieux, A. Ferrarini and G. P. Spada, *J. Am. Chem. Soc.*, 2001, **123**, 7842–7851.

22 K. Fukuda, H. Suzuki, J. Ni, M. Tokita and J. Watanabe, *Jpn. J. Appl. Phys.*, 2007, **46**, 5208–5212.
23 H. G. Kuball, B. Weiß, A. K. Beck and D. Seebach, *Helv. Chim. Acta*, 1997, **80**, 2507–2514.
24 S. Superchi, M. I. Donnoli, G. Proni, G. P. Spada and C. Rosini, *J. Org. Chem.*, 1999, **64**, 4762–4767.
25 G. Gottarelli, G. Proni, G. P. Spada, D. Fabbri, S. Gladiali and C. Rosini, *J. Org. Chem.*, 1996, **61**, 2013–2019.
26 K. Kishikawa, Y. Furukawa, T. Watanabe, M. Kohri, T. Taniguchi and S. Kohmoto, *Liq. Cryst.*, 2017, **44**, 969–988.
27 Y. Matsuoka, H. Sato, A. Yamagishi, K. Okamoto and N. Hoshino, *Chem. Mater.*, 2005, **17**, 4910–4917.
28 J. Yoshida, G. Watanabe, K. Kakizawa, Y. Kawabata and H. Yuge, *Inorg. Chem.*, 2013, **52**, 11042–11050.
29 A. Ferrarini, P. L. Nordio, P. V. Shibaev and V. P. Shibaev, *Liq. Cryst.*, 1998, **24**, 219–227.
30 K. Kakisaka, H. Higuchi, Y. Okumura and H. Kikuchi, *Chem. Lett.*, 2014, **43**, 624–625.
31 K. Kakisaka, H. Higuchi, Y. Okumura and H. Kikuchi, *J. Mater. Chem. C*, 2014, **2**, 6467–6470.
32 A. Bondi, *J. Phys. Chem.*, 1964, **68**, 441–451.
33 P. R. Wells, *Chem. Rev.*, 1963, **63**, 171–219.
34 A. Ferrarini, G. J. Moro and P. L. Nordio, *Mol. Phys.*, 1996, **87**, 485–499.
35 A. Ferrarini, G. J. Moro and P. L. Nordio, *Phys. Rev. E: Stat. Phys., Plasmas, Fluids, Relat. Interdiscip. Top.*, 1996, **53**, 681–688.
36 The K_{22} of JC-1041XX was provided by JNC Co.
37 A. Krekhov and W. Pesch, *Phys. Rev. E: Stat., Nonlinear, Soft Matter Phys.*, 2011, **83**, 051706-1–051706-13.
38 C. A. Hunter, K. R. Lawson, J. Perkins and C. J. Urch, *J. Chem. Soc., Perkin Trans. 2*, 2001, 651–669.
39 F. Cozzi, M. Cinquini, R. Annunziata, T. Dwyer and J. S. Siegel, *J. Am. Chem. Soc.*, 1992, **144**, 5729–5733.
40 S. Pieraccini, A. Ferrarini, K. Fuji and G. P. Spada, *Chirality*, 2008, **20**, 749–759.
41 H. Nishikawa, D. Mochizuki, H. Higuchi, Y. Okumura and H. Kikuchi, *ChemistryOpen*, 2017, **6**, 710–720.
42 H. Ishitani, M. Ueno and S. Kobayashi, *J. Am. Chem. Soc.*, 2000, **122**, 8180–8186.
43 M. Jahjah, M. Alame, S. P. Rostaing and M. Lemaire, *Tetrahedron: Asymmetry*, 2007, **18**, 2305–2312.
44 M. J. Frisch, G. W. Trucks, H. B. Schlegel, G. E. Scuseria, M. A. Robb, J. R. Cheeseman, G. Scalmani, V. Barone, B. Mennucci, G. A. Petersson, H. Nakatsuji, M. Caricato, X. Li, H. P. Hratchian, A. F. Izmaylov, J. Bloino, G. Zheng, J. L. Sonnenberg, M. Hada, M. Ehara, K. Toyota, R. Fukuda, J. Hasegawa, M. Ishida, T. Nakajima, Y. Honda, O. Kitao, H. Nakai, T. Vreven, J. A. Montgomery Jr, J. E. Peralta, F. Ogliaro, M. Bearpark, J. J. Heyd, E. Brothers, K. N. Kudin, V. N. Staroverov, T. Keith, R. Kobayashi, J. Normand, K. Raghavachari, A. Rendell, J. C. Burant, S. S. Iyengar, J. Tomasi, M. Cossi, N. Rega, J. M. Millam, M. Klene, J. E. Knox, J. B. Cross, V. Bakken, C. Adamo, J. Jaramillo, R. Gomperts, R. E. Stratmann, O. Yazyev, A. J. Austin, R. Cammi, C. Pomelli, J. W. Ochterski, R. L. Martin, K. Morokuma, V. G. Zakrzewski, G. A. Voth, P. Salvador, J. J. Dannenberg, S. Dapprich, A. D. Daniels, O. Farkas, J. B. Foresman, J. V. Ortiz, J. Cioslowski and D. J. Fox, *Gaussian 09, Revision D.01*, Gaussian, Inc., Wallingford CT, 2009.